ORIGINAL ARTICLE

A regularized solution for the inverse conductivity problem using mollifiers

Peter Maass[a], Michael Pidcock[b] and Cristiana Sebu[b]*

[a]*Zentrum für Technomathematik, Universität Bremen, Germany*; [b]*School of Technology, Oxford Brookes University, Oxford OX33 1HX, United Kingdom*

In this paper we present a reconstruction method for the inverse conductivity problem suitable for smooth conductivity distributions. The inverse problem is reformulated in terms of a pair of coupled integral equations, one of which is of first kind which we regularize using mollifier methods. An interesting feature of this method is that the kernel of this integral equation is not given, but can be modified for the choice of mollifier. We are able to obtain conductivity reconstructions rapidly and without relying on accurate *a priori* information.

Keywords: Inverse conductivity problem, Electrical Impedance Tomography, integral equation methods, mollifiers, nonlinear inverse problems, ill-posed problems.

AMS Subject Classification: 31B10, 45Q05, 45B05, 47A52.

1. Introduction

The inverse conductivity problem has attracted much attention and one of the main reasons is that although in its basic form the problem is relatively easy to state, it is extremely challenging mathematically. This is because it turns out to be both nonlinear and, above all, extremely ill-posed in the Hadamard sense. A further very positive aspect of the problem is that it has a practical realisation which is known as Electrical Impedance Tomography (EIT). This application which has its own substantial challenges in the fields of biomedical engineering and instrumentation, offers the possibility of a whole range of exciting and extremely useful applications in medical or industrial tomography at a very modest cost.

Substantial progress has been made in determining the class of conductivity distributions that can be recovered from the boundary data [1–5], as well as in designing practical reconstruction algorithms applicable to noisy measurement data. Reconstruction procedures addressing the full nonlinear problem include a wide range of iterative methods based on formulating the inverse problem in the framework of nonlinear optimisation. While these techniques are promising for obtaining accurate reconstructed conductivity values, they are often slow to converge and are quite demanding computationally particularly when addressing the three dimensional problem. These concerns have encouraged the search for reconstruction algorithms which reduce the computational demands. Some use *a priori* information to reconstruct piecewise constant conductivity distributions e.g. [6–8] while others

*Corresponding author. Email: csebu@brookes.ac.uk

are based on reformulating the inverse problems in terms of integral equations [9–14]. This list is by no means exhaustive and new approaches are constantly being presented [15].

In this paper we describe a reconstruction method suitable for smooth conductivity distributions. It uses a simple transformation to establish a connection between the equations defining the inverse conductivity problem and those used in Inverse Scattering [16]. By combining this process with the concept of mollifiers [17–21] we are able to obtain conductivity reconstructions for arbitrary geometry, extremely rapidly and without relying on accurate *a priori* information. This is achieved by reformulating the inverse problem in terms of a pair of coupled integral equations, one of which is of the first kind which we solve using mollifier methods. An interesting feature of this method is that the kernel of this integral equation is not given, but can be modified for the choice of mollifier.

The paper is organized as follows: Section 2 gives an outline of the basic reconstruction method. In Section 3 we describe the concept of mollifiers and discuss the advantages of this approach. In Section 4 we show how the technique described in Section 2 can be regularized using mollifiers and in Section 5 we discuss the choice of optimal boundary data. Section 6 contains the numerical experiments which indicate the possibilities and limitations of the combination of these two powerful theoretical tools.

2. The basic approach

Let $\Omega \subset \mathbb{R}^n$, $n = 2$ or 3, be a bounded simply connected domain with boundary $\partial\Omega \in C^2$ and let σ be an isotropic conductivity distribution in Ω, where $0 < c \leq \sigma < \infty$ and $\sigma \in C^2(\Omega) \cap C^1(\overline{\Omega})$. It is well known that if an electric current $j = \sigma \frac{\partial \Phi}{\partial n}$ is applied on $\partial\Omega$ then the induced electric potential Φ satisfies the equation

$$\nabla \cdot (\sigma(\mathbf{x}) \nabla \Phi(\mathbf{x})) = 0 \ , \ \mathbf{x} \in \Omega \ . \tag{1}$$

Using the well-known change of variables $\tau = \sqrt{\sigma}$ we can rewrite equation (1) in the form

$$\Delta \Psi(\mathbf{x}) = -V(\mathbf{x}) \Psi(\mathbf{x}) \ , \ \mathbf{x} \in \Omega, \tag{2}$$

where

$$V(\mathbf{x}) \ = \ -\frac{\Delta \tau(\mathbf{x})}{\tau(\mathbf{x})} \ , \tag{3a}$$

$$\Psi(\mathbf{x}) \equiv \tau(\mathbf{x})(\Phi(\mathbf{x}) + \Phi_0) \, , \tag{3b}$$

and Φ_0 is an arbitrary constant.

In this work we will assume that from data measurements on the boundary we have a knowledge of both σ and Φ and their normal derivatives on $\partial\Omega$. The inverse conductivity problem is to use this information to identify σ in Ω. Although it might seem that our inverse problem is overdetermined, we do not use all this information but only certain linear combinations. In terms of the new variables, the reconstruction problem becomes that of finding V (and consequently σ) from a knowledge of Ψ and $\frac{\partial \Psi}{\partial n}$ on $\partial\Omega$ which is a similar to the data normally used.

Definition 2.1: Suppose $\lambda : \Omega \to \mathbb{R}$ is bounded. Let $\mathcal{H} : \Omega \times \Omega \to \mathbb{R}$ be a bounded solution of the Schrödinger equation with respect to the second variable, i.e.

$$\Delta_{\mathbf{y}} \mathcal{H}(\mathbf{x}, \mathbf{y}) \; + \lambda(\mathbf{y})\, \mathcal{H}(\mathbf{x}, \mathbf{y}) \; = \; 0\,, \quad \mathbf{x}\,, \mathbf{y} \in \Omega\,. \tag{4}$$

Let $\mathcal{F}$ be the set of functions $f : \Omega \to \mathbb{R}$ which satisfy the Schrödinger equation

$$\Delta_{\mathbf{y}} f(\mathbf{y}) + \lambda(\mathbf{y}) f(\mathbf{y}) = 0\,, \quad \mathbf{y} \in \Omega\,. \tag{5}$$

Remark 1: Since $\mathcal{H}(\mathbf{x}, \cdot) \in L^\infty(\Omega)$ and $\mathcal{H}(\cdot, \mathbf{y}) \in H^2(\Omega)$, $\mathcal{H}$ is a function of Hilbert-Schmidt type.

We can apply Green's second identity [22, 23] to the functions Ψ and $\mathcal{H}$ defined above, and to Ψ and the free space Green's function for Schrödinger's equation (4), $\mathcal{G}_0(\mathbf{x}, \mathbf{y})$, to derive two integral representations of problem (2):

$$0 = \zeta(\mathbf{x}) - \int_\Omega d\mathbf{y}\; \mathcal{H}(\mathbf{x}, \mathbf{y}) X(\mathbf{y})\;,\; \mathbf{x} \in \Omega\;, \tag{6}$$

$$\Psi(\mathbf{x}) = \zeta_0(\mathbf{x}) + \int_\Omega d\mathbf{y}\; \mathcal{G}_0(\mathbf{x}, \mathbf{y}) X(\mathbf{y})\;,\; \mathbf{x} \in \Omega\;, \tag{7}$$

where

$$X(\mathbf{y}) = (V(\mathbf{y}) - \lambda(\mathbf{y}))\Psi(\mathbf{y})\,, \tag{8}$$

$$\zeta(\mathbf{x}) = \int_{\partial\Omega} d\mathbf{y}\; \left(\Psi(\mathbf{y}) \frac{\partial \mathcal{H}}{\partial n}(\mathbf{x}, \mathbf{y}) - \mathcal{H}(\mathbf{x}, \mathbf{y}) \frac{\partial \Psi(\mathbf{y})}{\partial n} \right)\;, \tag{9}$$

$$\zeta_0(\mathbf{x}) = \int_{\partial\Omega} d\mathbf{y}\; \left(\mathcal{G}_0(\mathbf{x}, \mathbf{y}) \frac{\partial \Psi(\mathbf{y})}{\partial n} - \Psi(\mathbf{y}) \frac{\partial \mathcal{G}_0}{\partial n}(\mathbf{x}, \mathbf{y}) \right)\;. \tag{10}$$

Remark 2: Note that the above formulation can also be applied to $\sigma \in W^{2,\infty}(\Omega)$. The reconstruction algorithm described below needs more care when applied to such weakly constrained conductivities and we will consider this in future work.

This integral equation formulation will allow us to develop a procedure for determining σ that is described in Section 3. It is important to note that since equation (6) is a Fredholm integral equation of the first kind, it is severely ill-posed and its solution has to be regularized. In this paper we examine the use of mollifiers to achieve this regularization. Finally, it is interesting to note that we have the possibility of choosing a function $\mathcal{H}(\mathbf{x}, \mathbf{y})$ which is either optimal in some sense or which has other desirable properties, yet to be determined.

3. A mollifier method for impedance tomography

Let us assume that σ, Ψ and $\frac{\partial \Psi}{\partial n}$ are known on $\partial\Omega$ and that an appropriate function $\mathcal{H}$ has been chosen. The reconstruction of σ in Ω using the formulation described in Section 2 then consists of four steps:

(1) Solve the linear problem $AX = \zeta$ (given by equation (6)) where

$$\begin{array}{rcl} A : L^2(\Omega) & \longrightarrow & L^2(\Omega) \\ X & \longmapsto & \int\limits_{\Omega} d\mathbf{y}\ \mathcal{H}(\mathbf{x},\mathbf{y})X(\mathbf{y})\,. \end{array} \tag{11}$$

The reconstructed $X(\mathbf{x})$ will be an approximation to $(V(\mathbf{x}) - \lambda(\mathbf{x}))\Psi(\mathbf{x})$, $\mathbf{x} \in \Omega$.

(2) Compute $\Psi(\mathbf{x})$ for $\mathbf{x} \in \Omega$ using a simple quadrature in equation (7).

(3) Compute $V(\mathbf{x})$ for $\mathbf{x} \in \Omega$ using equation (8)

$$V(\mathbf{x}) = \frac{X(\mathbf{x})}{\Psi(\mathbf{x})} + \lambda(\mathbf{x})\ . \tag{12}$$

Any computational difficulties related to very small or zero values of $\Psi(\mathbf{x})$ in Ω can be avoided by an appropriate choice of the constant Φ_0 defined in equation (3b).

(4) Compute $\tau(\mathbf{x}) = \sqrt{\sigma(\mathbf{x})}\ ,\ x \in \Omega$ by solving

$$\Delta\tau(\mathbf{x}) = -V(\mathbf{x})\tau(\mathbf{x})\ , \tag{13}$$

with given boundary values $\tau(\mathbf{x})$ and $\frac{\partial\tau}{\partial n}$, $\mathbf{x} \in \partial\Omega$.

Note that this procedure has transformed the non-linear ill-posed inverse conductivity problem into a linear ill-posed problem (step 1) followed by a non-linear process (step 3) leading to a unique stable solution of the partial differential equation (13) (step 4). Note also that once a regularized solution to equation (6) has been found, the conductivity distribution inside Ω will be uniquely reconstructed by following the remaining steps of the algorithm.

The solution of the ill-posed linear problem in step 1 can be stabilized using any regularization method for integral equations of the first kind. However, mollifier methods offer certain advantages as follows:

(i) Applications in medicine or geophysics will require different resolutions in different regions of Ω. This requirement might depend on the distance of the reconstruction point $\mathbf{x}$ from the measurement equipment or allow us to incorporate some *a priori* knowledge about homogeneous subregions. Locally adapted resolution can be easily incorporated in a mollifier approach.

(ii) The inversion of A is an ill-posed problem and data errors of ζ are amplified in the reconstruction. The mollifier approach overcomes this problem by requiring us to solve an operator equation for every reconstruction point $\mathbf{x}$ with an analytically given exact right hand side. This intermediate step can be precomputed with arbitrary precision.

(iii) Once the pointwise reconstruction vectors have been precomputed, the final data-dependent reconstruction step simply requires the computation of one scalar product per reconstruction point.

The mollifier method is a pointwise reconstruction technique [17–20] and is a generalization of the Backus and Gilbert method [24, 25]. It is based on a Dirac-sequence $\{e_\gamma(\widetilde{\mathbf{y}},\mathbf{y})\}$, such that

$$\int\limits_{\Omega} d\mathbf{y}\ e_\gamma(\widetilde{\mathbf{y}},\mathbf{y})X(\mathbf{y}) \longrightarrow \quad X(\widetilde{\mathbf{y}})\ ,\ \text{as}\ \gamma \to 0\ . \tag{14}$$

A standard choice of mollifier is given by

$$e_\gamma(\widetilde{\mathbf{y}},\mathbf{y}) = \frac{1}{|B(\widetilde{\mathbf{y}},\gamma)|}\cdot\chi_{B(\widetilde{\mathbf{y}},\gamma)}(\mathbf{y}) = \frac{1}{|B(\widetilde{\mathbf{y}},\gamma)|}\cdot\begin{cases}1:\mathbf{y}\in B(\widetilde{\mathbf{y}},\gamma)\\ 0:\text{otherwise}\end{cases} \tag{15}$$

and this is the one we use in this paper. The parameter γ is called the resolution or the regularization parameter at the point $\widetilde{\mathbf{y}}$ and $B(\widetilde{\mathbf{y}},\gamma)=\{\mathbf{y}:\ ||\widetilde{\mathbf{y}}-\mathbf{y}||\leq\gamma\}$.

Now assume that a reconstruction point $\widetilde{\mathbf{y}}$ and a desired resolution γ have been chosen. The value of γ may vary for different reconstruction points but we will suppress this dependence to simplify the notation in this paper. Instead of reconstructing X itself, we attempt a reconstruction of

$$X_\gamma(\widetilde{\mathbf{y}}) = \int\limits_\Omega d\mathbf{y}\ e_\gamma(\widetilde{\mathbf{y}},\mathbf{y})X(\mathbf{y})\ . \tag{16}$$

Since $\widetilde{\mathbf{y}}$ is fixed for the moment, we have

$$X_\gamma(\widetilde{\mathbf{y}}) =< e_\gamma(\widetilde{\mathbf{y}},\cdot), X >_{L^2(\Omega)}\ . \tag{17}$$

The adjoint operator A^* of the operator A defined in (11) is given by

$$\begin{aligned}A^*: L^2(\Omega)&\to L^2(\Omega)\\ u&\mapsto \int\limits_\Omega d\mathbf{x}\ \mathcal{H}(\mathbf{x},\mathbf{y})u(\mathbf{x})\ .\end{aligned}$$

The use of mollifier methods as a regularization technique was introduced in [17]. The basic idea is to find, at each reconstruction point $\widetilde{\mathbf{y}}$, a function $u_\gamma(\widetilde{\mathbf{y}},\cdot)$ satisfying

$$A^*u_\gamma(\widetilde{\mathbf{y}},\cdot) = e_\gamma(\widetilde{\mathbf{y}},\cdot) \tag{18}$$

or to compute a minimum norm approximation to $u_\gamma(\widetilde{\mathbf{y}},\cdot)$ by solving

$$min||A^*u_\gamma(\widetilde{\mathbf{y}},\cdot)-e_\gamma(\widetilde{\mathbf{y}},\cdot)||_{L^2(\Omega)}\ \text{ using }\ AA^*u_\gamma(\widetilde{\mathbf{y}},\cdot) = Ae_\gamma(\widetilde{\mathbf{y}},\cdot)\ . \tag{19}$$

We can then easily estimate

$$\begin{aligned}X_\gamma(\widetilde{\mathbf{y}}) &=< e_\gamma(\widetilde{\mathbf{y}},\cdot), X >_{L^2(\Omega)}\approx< A^*u_\gamma(\widetilde{\mathbf{y}},\cdot), X >_{L^2(\Omega)}=< u_\gamma(\widetilde{\mathbf{y}},\cdot), AX >_{L^2(\Omega)}\\ &=< u_\gamma(\widetilde{\mathbf{y}},\cdot),\zeta >_{L^2(\Omega)}\ .\end{aligned} \tag{20}$$

Consequently, the reconstruction at the point $\widetilde{\mathbf{y}}$ is achieved by simply computing a scalar product of the data ζ with the precomputed $u_\gamma(\widetilde{\mathbf{y}},\cdot)$. The construction of $u_\gamma(\widetilde{\mathbf{y}},\cdot)$ requires us to solve the ill-posed operator equation (18). However, this can be precomputed and -more important- the right hand side of equation (18) is known exactly.

4. The choice of mollifier

The choice of the mollifier will determine the quality of the reconstruction and its selection should reflect the properties of the operator as well as information

about the quality of the data. However, we have another degree of freedom in the reconstruction process described above: the choice of the function $\mathcal{H}$. In other words, the choice of the kernel of the integral operator is at our disposal. This is very different from the situation in standard linear inverse problems and will be the key element for our further investigations.

Let us begin with a discussion of the mollifier $e_\gamma(\widetilde{\mathbf{y}}, \mathbf{y})$, $\widetilde{\mathbf{y}}$, $\mathbf{y} \in \Omega$. Let $\tilde{e}_\gamma = A^* u_\gamma$, where u_γ is the minimizer of equation (19). This implies that we actually do not reconstruct

$$X_\gamma(\mathbf{x}) = \int_\Omega d\mathbf{y}\ X(\mathbf{y}) e_\gamma(\mathbf{x}, \mathbf{y})\,, \tag{21}$$

but rather

$$X_\gamma(\mathbf{x}) = \int_\Omega d\mathbf{y}\ X(\mathbf{y}) \widetilde{e}_\gamma(\mathbf{x}, \mathbf{y})\ . \tag{22}$$

In order to determine $\tilde{e}_\gamma$ we first need to determine the range of A^*. This range depends on the choice of the integral kernel $\mathcal{H}$.

Lemma 4.1: *Range* $(A^*) \subset \mathcal{F}$.

Proof: Consider $f \in L^2(\Omega)$, then it is straightforward to show that

$$\Delta_{\mathbf{y}} A^* f(\mathbf{y}) = -\lambda(\mathbf{y}) A^* f(\mathbf{y})\ .$$

□

Hence we can aim at best at an effective mollifier $\widetilde{e}_\gamma(\widetilde{\mathbf{y}}, \mathbf{y})$ which satisfies the Schrödinger equation (4) in $\mathbf{y}$.

Definition 4.2: We denote by

$$\{h_l(\mathbf{y}) \mid l \in \mathbb{Z}\} \tag{23}$$

an orthonormal basis for $\mathcal{F}$.

The effective mollifier at point $\widetilde{\mathbf{y}}$ is given by

$$\widetilde{e}_\gamma(\widetilde{\mathbf{y}}, \mathbf{y}) = \sum_{l \in \mathbb{Z}} < e_\gamma(\widetilde{\mathbf{y}}, \cdot), h_l >_{L^2(\Omega)}\ h_l(\mathbf{y})\ . \tag{24}$$

Since the range of a non-degenerate compact operator A^* is not closed, we still cannot ensure that (19) can be solved with e_γ replaced by $\tilde{e}_\gamma$. However, the kernel $\mathcal{H}$ of A^* is at our disposal and we can easily ensure $\widetilde{e}_\gamma(\widetilde{\mathbf{y}}, \mathbf{y}) \in \mathit{Range}(A^*)$ by choosing

$$\mathcal{H}(\mathbf{x}, \mathbf{y}) = \sum_{l \in \mathbb{Z}} c_l(\mathbf{x}) < e_\gamma(\widetilde{\mathbf{y}}, \cdot), h_l >_{L^2(\Omega)}\ h_l(\mathbf{y}) \tag{25}$$

with bounded coefficient functions $\{c_l(\mathbf{x})\}$ satisfying

$$|c_l(\mathbf{x})| \leq M_l\,, \quad \mathbf{x} \in \Omega\,, \quad \text{where} \quad \sum_{l \in \mathbb{Z}} M_l < \infty\,. \tag{26}$$

The computation of the reconstruction functional $u_\gamma(\widetilde{\mathbf{y}},\cdot)$ is now achieved using

$$A^* u_\gamma(\widetilde{\mathbf{y}},\mathbf{y}) = \int_\Omega d\mathbf{x}\ \mathcal{H}(\mathbf{x},\mathbf{y}) u_\gamma(\widetilde{\mathbf{y}},\mathbf{x})$$
$$= \sum_{l\in\mathbb{Z}} < e_\gamma(\widetilde{\mathbf{y}},\cdot), h_l >_{L^2(\Omega)} h_l(\mathbf{y}) \int_\Omega d\mathbf{x}\ c_l(\mathbf{x}) u_\gamma(\widetilde{\mathbf{y}},\mathbf{x})\ . \qquad (27)$$

Since $h_l \in H^2(\Omega)$, then by embedding theorems $h_l \in L^\infty(\Omega)$, and the validity of reversal of the summation and integration is guaranteed by the Weierstrass M-test [26]. The solvability of

$$A^* u_\gamma(\widetilde{\mathbf{y}},\cdot) \ = \ \widetilde{e}_\gamma(\widetilde{\mathbf{y}},\cdot)$$

gives another restriction on the kernel $\mathcal{H}$. Comparing equations (24) and (27) we can see that this equation is satisfied for any $\{c_l\}$ and u_γ provided

$$< c_l, u_\gamma(\widetilde{\mathbf{y}},\cdot) >_{L^2(\Omega)} = 1\ . \qquad (28)$$

Let us summarize the previous calculations.

Lemma 4.3: *For a fixed point $\widetilde{\mathbf{y}} \in \Omega$, let $e_\gamma(\widetilde{\mathbf{y}},\cdot) \in L^2(\Omega)$ denote a mollifier function, and $\widetilde{e}_\gamma(\widetilde{\mathbf{y}},\mathbf{y})$ its projection on $\mathcal{F}$ given by equation (24). Determine $u_\gamma(\widetilde{\mathbf{y}},\mathbf{x})$ and $\{c_l | l \in \mathbb{Z}\}$ satisfying equations (26) and (28).*

Choosing the kernel $\mathcal{H}(\mathbf{x},\mathbf{y})$, $\mathbf{x}$, $\mathbf{y} \in \Omega$, of A^* by

$$\mathcal{H}(\mathbf{x},\mathbf{y}) = \sum_{l\in\mathbb{Z}} c_l(\mathbf{x}) < e_\gamma(\widetilde{\mathbf{y}},\cdot), h_l >_{L^2(\Omega)} h_l(\mathbf{y})$$

leads to a reconstruction functional $u_\gamma(\widetilde{\mathbf{y}},\mathbf{x})$ such that

$$X_\gamma(\widetilde{\mathbf{y}}) = < AX, u_\gamma(\widetilde{\mathbf{y}},\cdot) >_{L^2(\Omega)} = \int_\Omega d\mathbf{y}\ X(\mathbf{y}) \widetilde{e}_\gamma(\widetilde{\mathbf{y}},\mathbf{y})\ .$$

We can simplify these calculations since for the actual computation we do not need to use the special choices of c_l and u_γ. In order to see this let us be more specific. Recall that we have as data

$$\Psi(\mathbf{x}) \ \text{ and } \ \frac{\partial \Psi}{\partial n}(\mathbf{x})\,, \quad \mathbf{x} \in \partial\Omega\ .$$

Theorem 4.4: *For a fixed point $\widetilde{\mathbf{y}} \in \Omega$, let $e_\gamma(\widetilde{\mathbf{y}},\mathbf{y}) \in L^2(\Omega)$ denote a mollifier function, and $\widetilde{e}_\gamma(\widetilde{\mathbf{y}},\mathbf{y})$ its projection on $\mathcal{F}$ given by equation (24). Then the mollified approximation to the solution X of equation (6) at $\widetilde{\mathbf{y}}$ is given by*

$$X_\gamma(\widetilde{\mathbf{y}}) \ = < X, \widetilde{e}_\gamma(\widetilde{\mathbf{y}},\cdot) >_{L^2(\Omega)} = \int_{\partial\Omega} \Big(\frac{\partial \widetilde{e}_\gamma}{\partial n}(\widetilde{\mathbf{y}},\mathbf{x}) \Psi(\mathbf{x}) - \widetilde{e}_\gamma(\widetilde{\mathbf{y}},\mathbf{x}) \frac{\partial \Psi}{\partial n}(\mathbf{x}) \Big) d\mathbf{x}\ . \qquad (29)$$

Proof: The right hand side of the integral equation (6) is given by

$$\zeta(\mathbf{x}) \;=\; \int\limits_{\partial\Omega} \Big(\frac{\partial \mathcal{H}}{\partial n}(\mathbf{x},\mathbf{y})\Psi(\mathbf{y}) - \mathcal{H}(\mathbf{x},\mathbf{y})\frac{\partial \Psi}{\partial n}(\mathbf{y})\Big) d\mathbf{y} \quad .$$

Hence we have to solve $AX = \zeta$. The reconstruction at $\widetilde{\mathbf{y}}$ is obtained by

$$X_\gamma(\widetilde{\mathbf{y}}) \;= < X, \widetilde{e}_\gamma(\widetilde{\mathbf{y}},\cdot) >_{L^2(\Omega)} = < \zeta, u_\gamma(\widetilde{\mathbf{y}},\cdot) >_{L^2(\partial\Omega)} \;\; .$$

Inserting the series expansion of $\mathcal{H}$, see (25), and the definition of ζ yields

$$X_\gamma(\widetilde{\mathbf{y}}) \;=\; \int\limits_{\Omega} d\mathbf{x}\; u_\gamma(\widetilde{\mathbf{y}},\mathbf{x}) \Bigg(\sum_{l\in\mathbb{Z}} < e_\gamma(\widetilde{\mathbf{y}},\cdot), h_l >_{L^2(\Omega)} c_l(\mathbf{x}) \int\limits_{\partial\Omega} \Big(\frac{\partial h_l}{\partial n}(\mathbf{y})\Psi(\mathbf{y}) - h_l(\mathbf{y})\frac{\partial \Psi}{\partial n}(\mathbf{y})\Big)\; d\mathbf{y} \Bigg) \; .$$

The integral over the variable $\mathbf{x}$ gives the value 1 independent of l, see (28). Hence interchanging summation and integration (again justified by the fact that $h_l \in H^2$ and using the Weierstrass M-test) gives the desired result. □

Remark 1: It is interesting to note that the calculation of the regularized solution X_γ at a point $\widetilde{\mathbf{y}} \in \Omega$ using equation (29) involves only an integration over the boundary $\partial\Omega$ and not the whole domain Ω. Moreover, the above theorem applies to any equation of the form (6). However, if in addition we assume that (6) is an integral formulation of equation (2) the result of Theorem 4.4 can be obtained with the use of Green's formula for the functions $\Psi(\mathbf{x})$ and $\widetilde{e}_\gamma(\widetilde{\mathbf{y}},\mathbf{x})$ as follows:

$$\int\limits_{\partial\Omega} \Big(\Psi(\mathbf{x})\frac{\partial \widetilde{e}_\gamma}{\partial n}(\widetilde{\mathbf{y}},\mathbf{x}) - \widetilde{e}_\gamma(\widetilde{\mathbf{y}},\mathbf{x})\frac{\partial \Psi}{\partial n}(\mathbf{x})\Big) d\mathbf{x} = \int\limits_{\Omega} \left(\Psi(\mathbf{x})\Delta\widetilde{e}_\gamma(\widetilde{\mathbf{y}},\mathbf{x}) - \widetilde{e}_\gamma(\widetilde{\mathbf{y}},\mathbf{x})\Delta\Psi(\mathbf{x})\right)\; d\mathbf{x}$$

$$= \int\limits_{\Omega} \left(-\lambda(\mathbf{x}) + V(\mathbf{x})\right) \Psi(\mathbf{x})\, \widetilde{e}_\gamma(\widetilde{\mathbf{y}},\mathbf{x})\; d\mathbf{x} \;=\; \int\limits_{\Omega} \; X(\mathbf{x})\, \widetilde{e}_\gamma(\widetilde{\mathbf{y}},\mathbf{x})\; d\mathbf{x} \;=\; X_\gamma(\widetilde{\mathbf{y}}) \, .$$

5. Choice of currents and voltages

The choice of $\mathcal{H}$ allows us to compute the projection of $X = (V-\lambda)\Psi$ in $\mathcal{F}$ from a single set of data measurements, namely $(\Psi, \frac{\partial\Psi}{\partial n})$. Hence, in general, we can achieve only a partial reconstruction of V and σ with one set of measurements, but several strategies for combining different measurements have been investigated, see for example [27].

However, there may be special cases where a single set of measurements is sufficient to recover σ.

Theorem 5.1: *If $X(\mathbf{x}) = (V(\mathbf{x}) - \lambda(\mathbf{x}))\,\Psi(\mathbf{x}) \in \mathcal{F}$ and if $\{\mathbf{x}\in\Omega | \Psi(\mathbf{x}) = 0\}$ has measure zero, then V and σ are determined completely from one measurement of Ψ and $\frac{\partial\Psi}{\partial n}$ on the boundary $\partial\Omega$.*

Proof: Let $\{h_l(\mathbf{x}) \mid l \in \mathbb{Z}\}$ be an orthonormal basis for $\mathcal{F}$. We now compute the

expansion coefficients of X for this basis. Using (2), integration by parts gives

$$\chi_l \equiv \int_\Omega h_l(\mathbf{x})X(\mathbf{x})d\mathbf{x} \;=\; \int_{\partial\Omega}\Big(\Psi(\mathbf{y})\frac{\partial h_l}{\partial n}(\mathbf{x}) - h_l(\mathbf{x})\frac{\partial\Psi(\mathbf{x})}{\partial n}\Big)d\mathbf{x}\;. \tag{30}$$

Since $X \in \mathcal{F}$ we can compute a full expansion $X(\mathbf{x}) = \sum_{l\in\mathbb{Z}} \chi_l h_l(\mathbf{x})$. Now we follow the reconstruction procedure described in Section 3 and obtain Ψ in all of Ω using (7). Our assumption on the zeros of Ψ allows us to determine $V(\mathbf{x}) = X(\mathbf{x})/\Psi(\mathbf{x}) + \lambda(\mathbf{x})$ almost everywhere. Subsequently τ and $\sigma = \tau^2$ are determined by (3a). □

The application of the above theorem requires the construction of a potential Φ such that $X = (V-\lambda)\Psi \in \mathcal{F}$. An applied current $j \in H^{-\frac{1}{2}}(\partial\Omega)$ induces a potential Φ and consequently Ψ on $\partial\Omega$. Using equation (30) we see that the optimal input current which makes the part of X in $\mathcal{F}$ as large as possible can be chosen as that which maximizes

$$\sum_{l\in\mathbb{Z}}|\chi_l|^2 \;=\; \sum_{l\in\mathbb{Z}}\left|\int_{\partial\Omega}\Big(\Psi(\mathbf{y})\frac{\partial h_l}{\partial n}(\mathbf{y}) - h_l(\mathbf{y})\frac{\partial\Psi(\mathbf{y})}{\partial n}\Big)d\mathbf{y}\;\right|^2 . \tag{31}$$

6. Further analytic development for constant λ

Although the analysis presented in the previous sections applies for any real valued function λ, the case of constant λ enables us to perform many of the calculations explicitly. Consequently, for the rest of this paper we will take λ to be a positive constant and hence the functions $\{h_l\}$ defined in (23) form an orthonormal set of solutions for the Helmholtz equation (4). The fundamental solution of equation (4) for $\lambda > 0$ is explicitly known for any dimension $n \geq 2$, see [28]. For example,

$$\mathcal{G}_0(\mathbf{x},\mathbf{y}) \;=\; \begin{cases} -\frac{1}{4}\,Y_0(\sqrt{\lambda}\,\|\mathbf{x}-\mathbf{y}\|) & n=2\,,\\[2ex] \frac{1}{4\pi}\,\frac{\cos(\sqrt{\lambda}\,\|\mathbf{x}-\mathbf{y}\|)}{\|\mathbf{x}-\mathbf{y}\|} & n=3\,, \end{cases}$$

where Y_0 is the Bessel function of the second kind.

Lemma 6.1: *For a given domain $\Omega \subset \mathbb{R}^n$, the function $\widetilde{e}_\gamma$ defined in equation (24) becomes*

$$\widetilde{e}_\gamma(\widetilde{\mathbf{y}},\mathbf{y}) = C(\gamma,\lambda)\sum_{l\in\mathbb{Z}} h_l(\widetilde{\mathbf{y}})h_l(\mathbf{y})\,. \tag{32}$$

Proof: The inner product $< e_\gamma(\widetilde{\mathbf{y}},\cdot), h_l >_{L^2(\Omega)}$ is given by

$$< e_\gamma(\widetilde{\mathbf{y}},\cdot), h_l >_{L^2(\Omega)} = \int_\Omega d\mathbf{y}\, e_\gamma(\widetilde{\mathbf{y}},\mathbf{y})h_l(\mathbf{y}) = \frac{1}{|B(\widetilde{\mathbf{y}},\gamma)|}\int_{B(\widetilde{\mathbf{y}},\gamma)} d\mathbf{y}\, h_l(\mathbf{y})\,. \tag{33}$$

Using the Mean Value Theorem for the Helmholtz equation [29] we can show that

$$\int_{B(\widetilde{\mathbf{y}},\gamma)} d\mathbf{y} h_l(\mathbf{y}) = \left(\frac{2\pi\gamma}{\sqrt{\lambda}}\right)^{\frac{n}{2}} J_{\frac{n}{2}}(\sqrt{\lambda}\gamma) h_l(\widetilde{\mathbf{y}})\,. \tag{34}$$

It follows that

$$< e_\gamma(\widetilde{\mathbf{y}},\cdot), h_l >_{L^2(\Omega)} = C(\gamma,\lambda) h_l(\widetilde{\mathbf{y}})\,, \tag{35}$$

where $C(\gamma,\lambda) = \left(\frac{2}{\sqrt{\lambda}\gamma}\right)^{\frac{n}{2}} \Gamma\Big(\frac{n}{2}+1\Big) J_{\frac{n}{2}}(\sqrt{\lambda}\gamma)$. Therefore,

$$\widetilde{e}_\gamma(\widetilde{\mathbf{y}},\mathbf{y}) = C(\gamma,\lambda) \sum_{l\in\mathbb{Z}} h_l(\widetilde{\mathbf{y}}) h_l(\mathbf{y})\,. \tag{36}$$

□

Lemma 6.2: *If $\lambda \to 0$ then equation (4) reduces to Laplace's equation and it is straightforward to show that $C(\gamma,\lambda) \to 1$. In other words the scalar product (35) is independent of the regularization parameter γ. Hence, the effective mollifier $\widetilde{e}_\gamma(\widetilde{\mathbf{y}},\mathbf{y})$ in (24) and, consequently, the reconstructed X_γ in (29) are independent of the resolution γ.*

If we restrict ourselves to simple geometries further explicit calculations are possible.

Lemma 6.3: *Let Ω be a two dimensional disk of radius R, $\Omega = \{\mathbf{y} = (r\cos\theta,\, r\sin\theta) \in \mathbb{R}^2 : \|\mathbf{y}\| \le R\ \}$, the orthonormal solutions $\left\{h_l^j : l \in \mathbb{Z}\,, j = 1,2\right\}$ of equation (4) for $\lambda > 0$ are given by*

$$h_l^1(r,\theta) = \rho_l J_l(\sqrt{\lambda}r)\cos(l\theta) = \rho_l \Re\left[J_l(\sqrt{\lambda}r)e^{il\theta}\right], \tag{37}$$

$$h_l^2(r,\theta) = \rho_l J_l(\sqrt{\lambda}r)\sin(l\theta) = \rho_l \Im\left[J_l(\sqrt{\lambda}r)e^{il\theta}\right], \tag{38}$$

where ρ_l are the normalization constants

$$\rho_l = \frac{1}{R}\sqrt{\frac{(2-\delta_{l0})}{\pi\left(J_l^2(\sqrt{\lambda}R) - J_{l-1}(\sqrt{\lambda}R)J_{l+1}(\sqrt{\lambda}R)\right)}}\,. \tag{39}$$

Hence,

$$\widetilde{e}_\gamma(\alpha,\psi;r,\theta) = \frac{2}{\sqrt{\lambda}\gamma} J_1(\sqrt{\lambda}\gamma) \sum_{l\in\mathbb{Z}} \rho_l^2 J_l(\sqrt{\lambda}\alpha) J_l(\sqrt{\lambda}r)\cos(l(\psi-\theta))\,, \tag{40}$$

where (α,ψ) are the polar coordinates of $\widetilde{\mathbf{y}}$, the centre of the mollifier disk. Furthermore, if the boundary data are sufficiently smooth to guarantee that $\Psi \in C(\partial\Omega)$,

and both Ψ' *and* $\frac{\partial\Psi}{\partial n}$ *are piecewise smooth on* $\partial\Omega$*, then*

$$X_\gamma(\alpha,\psi) = \frac{2\pi R J_1(\sqrt{\lambda}\gamma)}{\sqrt{\lambda}\gamma}\sum_{l\in\mathbb{Z}}\rho_l^2\ J_l(\sqrt{\lambda}\alpha)\Big[\big(a_l\cos(l\psi)+b_l\sin(l\psi)\big)J_l'(\sqrt{\lambda}R) - \big(c_l\cos(l\psi)+d_l\sin(l\psi)\big)J_l(\sqrt{\lambda}R)\Big], \qquad (41)$$

where a_l,b_l *and* c_l,d_l *are the Fourier series coefficients of* $\Psi(R,\theta)$ *and* $\frac{\partial\Psi}{\partial n}(R,\theta)$*, respectively.*

Proof: It is straightforward to show that $J_l(\sqrt{\lambda}r)e^{il\theta}$ are orthogonal solutions to equation (4). In order to guarantee an orthonormal set of solutions $\{h_l\}$ we require that

$$\int_\Omega d\mathbf{y}\, h_l^j(\mathbf{y})^2 \;=\; \rho_l^2\pi\int_0^R dr\, r J_l(\sqrt{\lambda}r)^2 \;=\; 1$$

and the result given in equation (39) follows. We can now derive the result for X_γ by substituting in equation (29) the explicit formula for $\widetilde{e}_\gamma$ given in equation (40). The smoothness assumptions on Ψ, Ψ' and $\frac{\partial\Psi}{\partial n}$ on the boundary $\partial\Omega$ imply that the Fourier coefficients a_l, $b_l \sim \frac{1}{l^{2+\epsilon}}$, and c_l, $d_l \sim \frac{1}{l^{1+\epsilon}}$, where $\epsilon > 0$ [26]. From the asymptotic behaviour of Bessel functions, it is straightforward to show that for large l

$$a_l\rho_l^2 J_l(\sqrt{\lambda}\alpha)J_l'(\sqrt{\lambda}R) \sim \Big(\frac{\alpha}{R}\Big)^l\frac{1}{l^\epsilon}, \quad \text{and} \quad c_l\rho_l^2 J_l(\sqrt{\lambda}\alpha)J_l(\sqrt{\lambda}R) \sim \Big(\frac{\alpha}{R}\Big)^l\frac{1}{l^\epsilon}.$$

Similar results hold for the terms involving b_l and d_l.

□

7. Numerical implementation on the unit disk

The results of Section 5 suggest that we should be able to use our method to determine an acceptable reconstruction from one measurement only. In principle, this requires an optimal choice of the induced current but in this paper we will investigate what can be reconstructed from a single measurement resulting from a standard pattern for the applied current.

The method described in this paper is not restricted to particular geometries, but for simplicity, as in the previous section, we consider the unit disk $\Omega = \{\mathbf{y} = (r\cos\theta,\, r\sin\theta) \in \mathbb{R}^2 \;:\; \|\mathbf{y}\| \le 1\ \}$. Our general procedure for performing the numerical test is as follows. We start by choosing a conductivity σ that we attempt to reconstruct. To simulate the measured values of the potential on the boundary we have first to solve the direct problem, and in order to avoid inverse crimes we use as forward solver the PDE Toolbox of Matlab which has no connection with the reconstruction method under consideration. Thus, we obtain Φ and Ψ as well as their normal derivatives at 214 equally spaced mesh points on the boundary.

The inversion algorithm is to use our mollifier method to compute X by means of equation (41) and then follow the step by step procedure described in Section

3. Once X is known the calculation of Ψ inside the unit disk is straightforward:

$$\Psi(r,\,\theta) = \zeta_0(r,\,\theta) + \int_0^1 d\rho\,\rho \int_0^{2\pi} d\vartheta \mathcal{G}_0(r,\,\theta;\,\rho,\,\vartheta) X(\rho,\,\vartheta)\,. \tag{42}$$

The function ζ_0 is computed numerically from the boundary data using the Composite Trapezium rule:

$$\zeta_0(r,\,\theta) = \int_0^{2\pi} d\vartheta \,\left(\mathcal{G}_0(r,\,\theta;\,1,\,\vartheta)\frac{\partial\Psi}{\partial n}(1,\,\vartheta) - \Psi(1,\,\vartheta)\frac{\partial\mathcal{G}_0}{\partial n}(r,\,\theta;\,1,\,\vartheta)\right)\,.$$

In order to compute the integral on the right-hand side of equation (42) we note that the integral kernel $\mathcal{G}_0$ has a weak singularity when $(r,\,\theta) = (\rho,\,\vartheta)$. However, this possible difficulty can be overcome by using special quadrature methods [30] or a subtraction technique [31] as follows:

$$\begin{aligned}\Psi(r,\,\theta) = \zeta_0(r,\,\theta) &+ \int_0^1 d\rho\,\rho \int_0^{2\pi} d\vartheta\,\mathcal{G}_0(r,\,\theta;\,\rho,\,\vartheta)\,[X(\rho,\,\vartheta) - X(r,\,\theta)] \\ &+ X(r,\,\theta)\int_0^1 d\rho\,\rho \int_0^{2\pi} d\vartheta\,\mathcal{G}_0(r,\,\theta;\,\rho,\,\vartheta).\end{aligned} \tag{43}$$

Since

$$\int_0^1 d\rho\,\rho \int_0^{2\pi} d\vartheta\,\mathcal{G}_0(r,\,\theta;\,\rho,\,\vartheta) \;=\; -\left(\frac{1}{\lambda} + \frac{\pi}{2\sqrt{\lambda}} J_0(\sqrt{\lambda}r)Y_1(\sqrt{\lambda})\right)\,,$$

relation (43) can be further simplified

$$\begin{aligned}\Psi(r,\,\theta) = \zeta_0(r,\,\theta) \;-\; X(r,\,\theta)&\left(\frac{1}{\lambda} + \frac{\pi}{2\sqrt{\lambda}} J_0(\sqrt{\lambda}r)Y_1(\sqrt{\lambda})\right) \\ &+ \sum_{k=1}^{172} w_k\,\mathcal{G}_0(r,\,\theta;\,\rho_k,\,\vartheta_k)\,[X(\rho_k,\,\vartheta_k) - X(r,\,\theta)]\,,\end{aligned}$$

where $\{\rho_k,\,\vartheta_k;\,w_k\}$ is a set of 172 quadrature points and weights for the unit disk given by Engels in [32]. V is then computed by means of equation (12). Equation (13) can be solved for τ in a stable way, for instance, by means of a Fredholm equation of the second kind with a weakly singular kernel:

$$\tau(r,\,\theta) = \tau_0(r,\,\theta) + \int_0^1 d\rho\,\rho \int_0^{2\pi} d\vartheta \mathcal{G}_0(r,\,\theta;\,\rho,\,\vartheta) V(\rho,\,\vartheta)\tau(\rho,\,\vartheta)\,, \tag{44}$$

where the function τ_0 is computed numerically from the boundary data again using

the Composite Trapezium rule:

$$\tau_0(r,\,\theta) = \int_0^{2\pi} d\vartheta \,\left(\mathcal{G}_0(r,\,\theta;\,1,\,\vartheta)\frac{\partial\tau}{\partial n}(1,\,\vartheta) - \tau(1,\,\vartheta)\frac{\partial\mathcal{G}_0}{\partial n}(r,\,\theta;\,1,\,\vartheta)\right) .$$

Using the same subtraction technique [31], equation (44) becomes

$$\begin{aligned}\tau(r,\,\theta) = \tau_0(r,\,\theta) \;-\; & V(r,\,\theta)\tau(r,\,\theta)\left(\frac{1}{\lambda} + \frac{\pi}{2\sqrt{\lambda}}J_0(\sqrt{\lambda}r)Y_1(\sqrt{\lambda})\right) \\ & + \sum_{k=1}^{172} w_k\,\mathcal{G}_0(r,\,\theta;\,\rho_k,\,\vartheta_k)\left[V(\rho_k,\,\vartheta_k)\tau(\rho_k,\,\vartheta_k) - V(r,\,\theta)\tau(r,\,\theta)\right] ,\end{aligned}$$

which can be reduced to a system of linear equations for the values of the function τ at the integration points $(\rho_i,\,\vartheta_i)$, $i = 1,\,2,\,\ldots,\,172$:

$$\begin{aligned}\tau_0(\rho_i,\,\vartheta_i) \;=\; & \tau(\rho_i,\,\vartheta_i) \;+\; V(\rho_i,\,\vartheta_i)\tau(\rho_i,\,\vartheta_i)\left(\frac{1}{\lambda} + \frac{\pi}{2\sqrt{\lambda}}J_0(\sqrt{\lambda}\rho_i)Y_1(\sqrt{\lambda})\right) \\ & - \sum_{k=1,\,k\neq i}^{172} w_k\,\mathcal{G}_0(\rho_i,\,\vartheta_i;\,\rho_k,\,\vartheta_k)\left[V(\rho_k,\,\vartheta_k)\tau(\rho_k,\,\vartheta_k) - V(\rho_i,\,\vartheta_i)\tau(\rho_i,\,\vartheta_i)\right] .\end{aligned}$$

The above system can be solved using LU decomposition or any other appropriate numerical technique [31]. To find the values of the function τ at any point of coordinates $(r,\,\theta)$ we cannot employ the usual Nyström continuation since our integral kernel $\mathcal{G}_0V$ in equation (44) becomes very large if the point $(r,\,\theta)$ is close to a quadrature point (ρ_k, ϑ_k). In order to overcome this problem, we use a modified Nyström continuation

$$\begin{aligned}\tau(r,\,\theta) = \tau_0(r,\,\theta) \;-\; & V(r,\,\theta)\tau(\rho_l,\vartheta_l)\left(\frac{1}{\lambda} + \frac{\pi}{2\sqrt{\lambda}}J_0(\sqrt{\lambda}r)Y_1(\sqrt{\lambda})\right) \\ & + \sum_{k=1}^{172} w_k\,\mathcal{G}_0(r,\,\theta;\,\rho_k,\,\vartheta_k)\left[V(\rho_k,\,\vartheta_k)\tau(\rho_k,\,\vartheta_k) - V(r,\,\theta)\tau(\rho_l,\,\vartheta_l)\right] ,\end{aligned}$$

where $(\rho_l,\,\vartheta_l)$ is the closest quadrature point to $(r,\,\theta)$.

8. Numerical examples

In the following numerical examples we present reconstruction results for data with 1% random errors and $\lambda = 1$. A noise level of 1% is reasonable in many circumstances but in some medical applications greater accuracy can be achieved [33]. In order to avoid any damping effects in the determination of V using equation (12) the value of λ cannot be large. Numerical experiments showed that a value of $\lambda = 1$ is an appropriate choice. Since the reconstruction is achieved extremely rapidly for any value of the resolution parameter γ, there is no benefit in using an adaptive resolution. Therefore we are able to use the same resolution $\gamma = 0.1$ for all reconstruction points. The optimal choice for the regularization parameter, γ, as given by the L-curve criterion, is approximately 0.1. This is in agreement with

the theoretical minimum spatial resolution achievable using our integral equation approach which was derived in [34].

Example 8.1 As a first example we attempt to reconstruct a conductivity distribution consisting of an off-centered high conductivity region within a constant background, see Figure 1(a),

$$\sigma_1(x,y) = 1 + \frac{1}{(x+0.7)^2 + (y+0.2)^2 + 0.1}\,.$$

We present in Figures 1(b), 1(c), 1(d) the reconstructed conductivity for data with 1% random errors and different input currents.

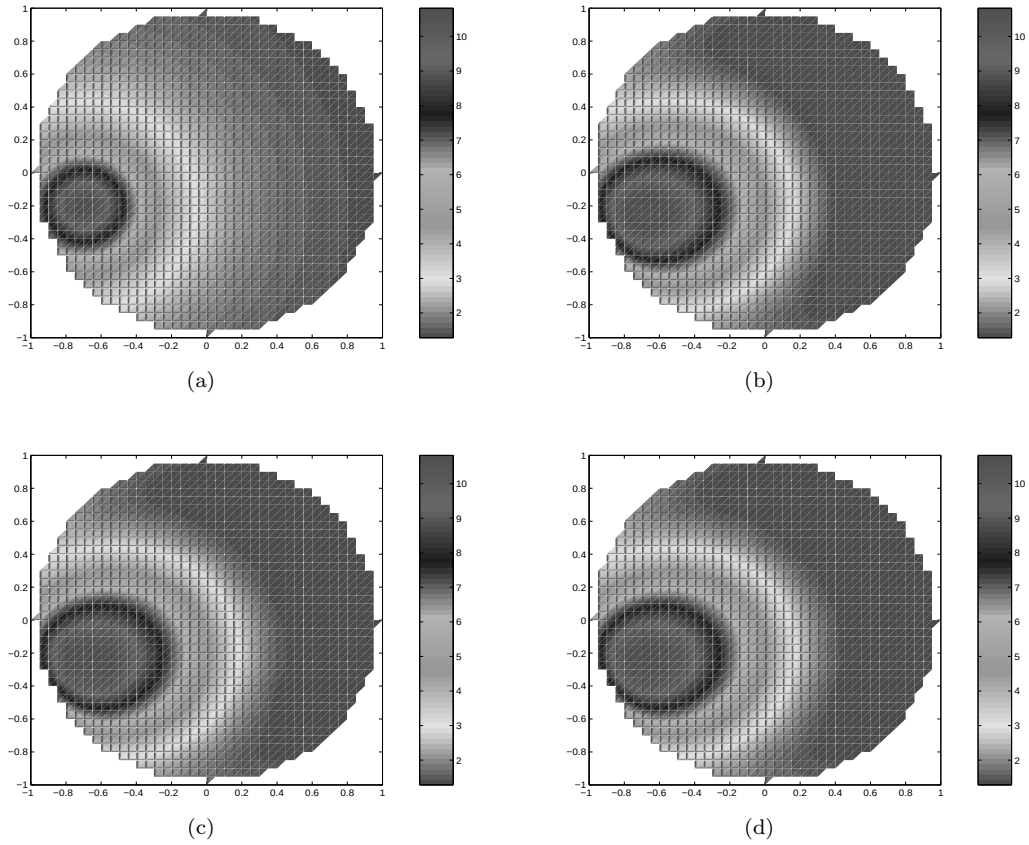

Figure 1. (a) The conductivity distribution $\sigma_1(x,y)$; The reconstructed conductivity, $\sigma_1^{reg}(x,y)$, for data with 1% errors: (b) $j(\theta) = \cos(\theta)$, $\|\sigma_1^{reg} - \sigma_1\|_{L^2} = 0.62$; (c) $j(\theta) = \cos(2\theta)$, $\|\sigma_1^{reg} - \sigma_1\|_{L^2} = 0.65$; (d) $j(\theta) = \sin(\theta)$, $\|\sigma_1^{reg} - \sigma_1\|_{L^2} = 0.63$.

Example 8.2 In the second example we consider a conductivity distribution consisting of two regions, one of high conductivity and one of low conductivity, see Figure 2(a),

$$\sigma_2(x,y) = 6 + \frac{1}{(x-0.6)^2 + (y-0.3)^2 + 0.1} - \frac{0.9}{(x+0.4)^2 + (y+0.5)^2 + 0.2}\,.$$

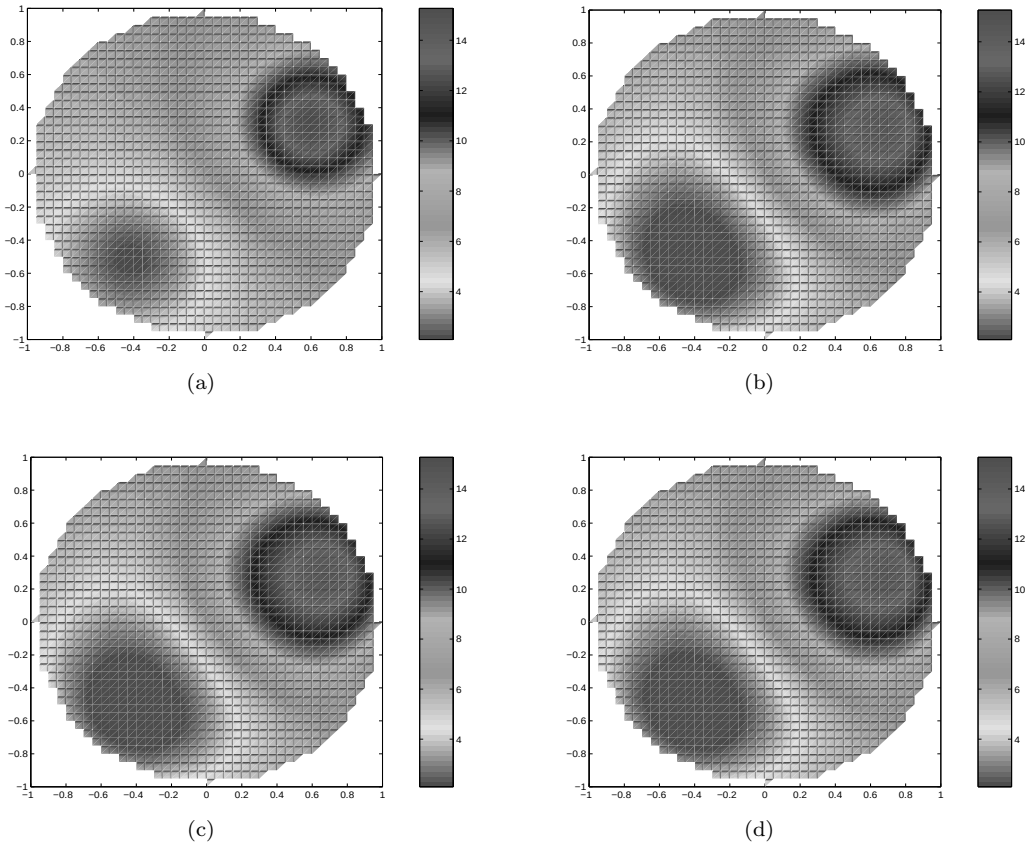

(a) (b) (c) (d)

Figure 2. (a) The conductivity distribution $\sigma_2(x, y)$; The reconstructed conductivity, $\sigma_2^{reg}(x, y)$, for data with 1% errors: (b) $j(\theta) = \cos(\theta)$, $\|\sigma_2^{reg} - \sigma_2\|_{L^2} = 1.33$; (c) $j(\theta) = \cos(2\theta)$, $\|\sigma_2^{reg} - \sigma_2\|_{L^2} = 1.39$; (d) $j(\theta) = \sin(\theta)$, $\|\sigma_2^{reg} - \sigma_2\|_{L^2} = 1.35$.

Example 8.3 In the third example we reconstruct a conductivity distribution consisting of two high conductivity regions, see Figure 3(a),

$$\sigma_3(x, y) = 1 + \frac{1}{(x - 0.7)^2 + y^2 + 0.1} + \frac{2}{(x + 0.6)^2 + y^2 + 0.2}\,.$$

In our numerical experiments, the location of the significant features was well determined but the reconstructed conductivities were smoother than the targets. We also found that the reconstruction algorithm is stable with respect to noise in the input data for error levels of up to 5%. In Figure 4 we plot the L^2-relative error, $e_{rel} = \|\sigma_2^{reg} - \sigma_2\|_{L^2}/\|\sigma_2\|_{L^2}$, as a function of noise level ε for the conductivity distribution considered in Example 8.2 and input current $j(\theta) = \cos(\theta)$.

9. Conclusion

In this paper we have investigated an application of mollifiers to the inverse conductivity problem. It is based on an assumed knowledge of the boundary values of the conductivity σ and of the potential Φ and their normal derivatives. We reformulate the inverse problem as a linear Fredholm integral equation of the first kind, where the kernel is not given, but can be chosen in a number of ways. The linear problem is efficiently solved by applying the method of mollifiers. Our algorithm allows us to choose an optimal regularization, and since we use the free space Green's func-

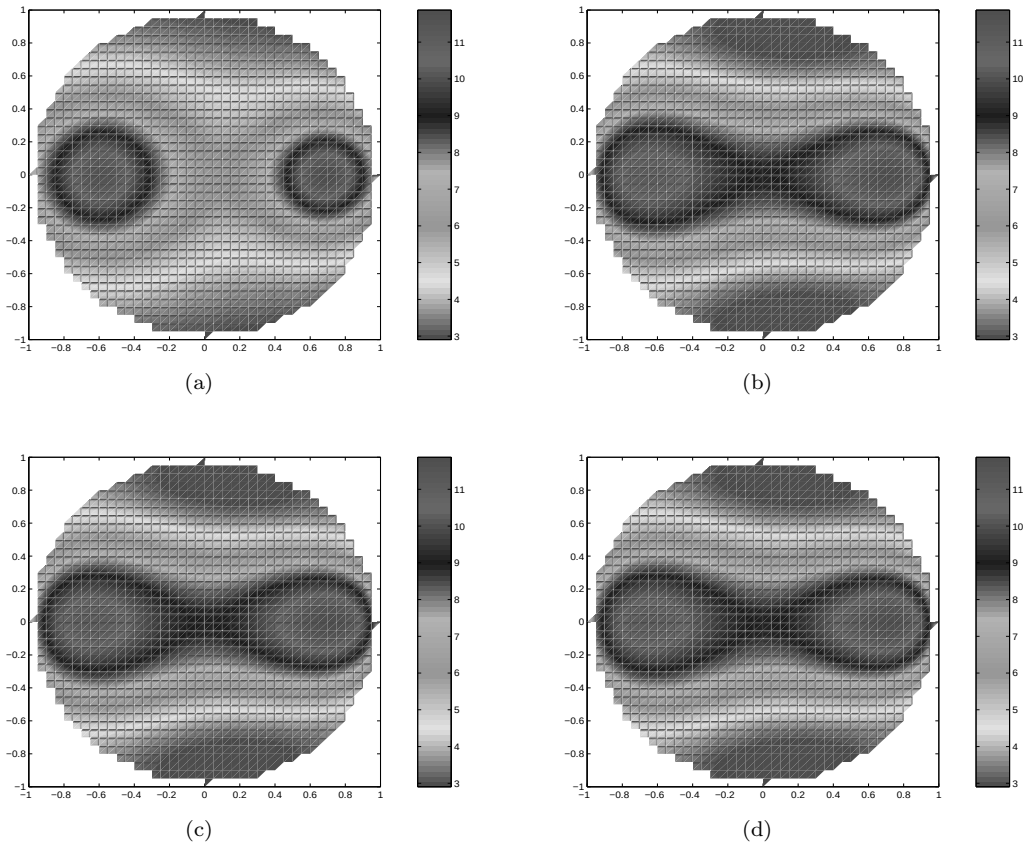

Figure 3. (a) The conductivity distribution $\sigma_3(x,y)$; The reconstructed conductivity, $\sigma_3^{reg}(x,y)$, for data with 1%: (b) $j(\theta)=\cos(\theta)$, $\|\sigma_3^{reg}-\sigma_3\|_{L^2}=1.48$; (c) $j(\theta)=\cos(2\theta)$, $\|\sigma_3^{reg}-\sigma_3\|_{L^2}=1.50$; (d) $j(\theta)=\sin(\theta)$, $\|\sigma_3^{reg}-\sigma_3\|_{L^2}=1.48$.

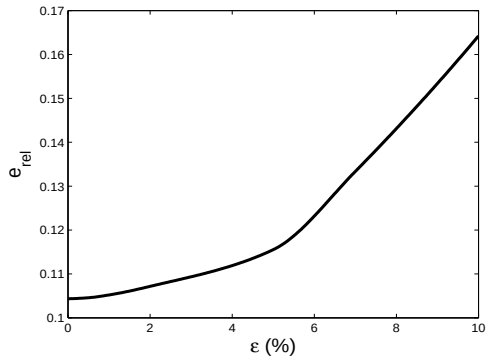

Figure 4. The L^2-relative error, $e_{rel}=\|\sigma_2^{reg}-\sigma_2\|_{L^2}/\|\sigma_2\|_{L^2}$, as a function of noise level ε for the conductivity distribution considered in Example 8.2 and input current $j(\theta)=\cos(\theta)$.

tion the approach is not geometrically constrained and can be applied to any two or three dimensional simply connected domain. Both the theoretical investigations and the numerical experiments indicate that the algorithm gives good reconstructions of smooth conductivity distributions, and that it is quite stable with respect to noise in the input data.

References

[1] A. P. Calderón, *Seminar on Numerical Analysis and its Applications to Continuum Physics*, Soc. Brasileira de Matemàtica, Rio de Janeiro, 1980, pp. 65–73.

[2] R. Kohn and M. S. Vogelius, *Determining conductivity by boundary measurements II. Interior results*, Comm. Pure Appl. Math. 38 (1985), pp. 643–667.

[3] J. Sylvester and G. Uhlmann, *Inverse boundary value problems at the boundary - Continuous dependence*, Comm. Pure Appl. Math, 41 (1988), pp. 197–221.

[4] A. I. Nachman, *Global uniqueness for a two-dimensional inverse boundary problem*, Ann. Math. 142 (1995), pp. 71–96.

[5] K. Astala and L. Païvärinta, *Calderon's inverse conductivity problem in plane*, Ann. Math. 163 (2006), pp. 265–299.

[6] D.J. Cedio-Fenygya, S. Moscow and M. S. Vogelius, *Identification of conductivity imperfections of small diameter by boundary measurements. Continuous dependence and computational reconstruction*, Inverse Problems 14 (1998), pp. 553–594.

[7] M. Brühl and M. Hanke, *Numerical implementation of two noniterative methods for locating inclusions by impedance tomography*, Inverse Problems 16 (2000), pp. 1029–1042.

[8] M. Brühl, M. Hanke and M. Vogelius, *A direct impedance tomography algorithm for locating small inhomogeneities*, Numer. Math. 93 (2003), pp. 635–654.

[9] S. Siltanen, J. Mueller and D. Isaacson, *An implementation of the reconstruction algorithm of A Nachman for the 2D inverse conductivity problem*, Inverse Problems 16 (2000), pp. 681–699.

[10] J. L. Mueller and S. Siltanen, *Direct reconstructions of conductivities from boundary measurements*, SIAM J. Sci. Comp. 24 (2003), pp. 1232–1266.

[11] R. Kress and W. Rundell, *Nonlinear integral equations and their iterative solution for an inverse boundary value problem*, Inverse Problems 21 (2005), pp. 1207–1223.

[12] S. Ciulli, M. Pidcock, T.D. Spearman and A. Stroian, *Image reconstruction in electrical impedance tomography using an integral equation of the Lippmann-Schwinger type*, Phys. Lett. A 271 (2000), pp. 377–384.

[13] S. Ciulli, M. Pidcock and C. Sebu,*On the inverse conductivity problem in the half space*, Z. Angew. Math. Mech. 83 (2003), pp. 755–765.

[14] S. Ciulli, M. K. Pidcock and C. Sebu, *An integral equation method for the inverse conductivity problem*, Phys. Lett. A 325 (2004), pp. 253–267.

[15] L. Borcea, *Electrical impedance tomography*, Inverse Problems 18 (2002), pp. R99–R136.

[16] D. Colton and R. Kress, *Inverse Acoustic and Electromagnetic Scattering Theory*, 2nd ed., Springer-Verlag, 1998.

[17] A. K. Louis and P. Maass, *A mollifier method for linear operator equations of the first kind*, Inverse Problems 6 (1990), pp. 427–440.

[18] A. K. Louis, *Approximate inverse for linear and some nonlinear problems*, Inverse Problems 12 (1996), pp. 175–190.

[19] A.K. Louis, *Inverse und Schlecht Gestellte Probleme*, Teubner, Stuttgart, 1989.

[20] A.K. Louis, *A unified approach to regularization methods for linear ill-posed problems*, Inverse Problems 15 (1999), pp. 489–498.

[21] H. Abdullah and A. Louis, *The approximate inverse for solving an inverse scattering problem for acoustic waves in an inhomogeneous medium*, Inverse Problems 15 (1999), pp. 1213–1230.

[22] J. L. Lions and E. Magenes, *Non-homogeneous Boundary Value Problems*, Vol. I, P. Kenneth (Transl.), Springer- Verlag, New York, 1972.

[23] C. Baiocchi and A. Capelo, *Variational and Quasivariational Inequalities. Applications to Free Boundary Problems*, John Wiley & Sons, Inc., New-York, 1984.

[24] G. Backus and F. Gilbert, *Numerical applications of a formalism for geophysical inverse problems*, Geophys. J. Royal Astron. Soc. 13 (1967), pp. 247–276.

[25] G.Backus and F. Gilbert, *The resolving power of gross Earth data*, Geophys. J. Royal Astron. Soc. 16 (1968), pp. 169–205.

[26] M. H. Protter and C. B. Morrey, *Modern Mathematical Analysis*, Addison-Wesley, Reading, Massachusetts, 1964.

[27] E. Wallacher, *Äquivalente Quellen als Zugang zur Lösung eines inverse Streuproblems*, Diplomarbeit, Universität des Saarlandes, 2002.

[28] J. Kervokian, *Partial Differential Equations. Analytical Solutions Techniques*, Texts in Applied Mathematics 35, 2nd ed., Springer Verlag, New York, 2000.

[29] R. Courant and D. Hilbert, *Methods of Mathematical Physics* Vol II, John Wiley & Sons, New York, 1989.

[30] R. Kress, *Linear Integral Equations*, Applied Mathematical Sciences 82, 2nd ed., Springer Verlag, New York, 1999.

[31] W. H Press, S. A. Teukolski, W. T. Vetterling and B. P. Flanerry, *Numerical Recipies in Fortran*, 2nd ed., Cambridge University Press, Cambridge, 1992.

[32] H. Engels, *Numerical Quadratures and Cubatures*, Academic Press, London, 1980.

[33] N. Terzopoulos, K. Hayatleh, B. Hart, F. J. Lidgey and C. McLeod, *A novel bipolar-drive circuit for medical applications*, Phys. Meas. 26 (2005), pp. N1-N7.

[34] P. C. Sabatier and C. Sebu, *On the resolving power of Electrical Impedance Tomography*, Inverse Problems 23 (2007), pp. 1895-1913.